Graphene Activating Room-Temperature Ferromagnetic Exchange in Cobalt-Doped ZnO Dilute Magnetic Semiconductor Quantum Dots

Zhihu Sun,[†] Xiaoyu Yang,[†] Chao Wang, Tao Yao, Liang Cai, Wensheng Yan,[*] Yong Jiang, Fengchun Hu, Jingfu He, Zhiyun Pan, Qinghua Liu,[*] and Shiqiang Wei[*]

National Synchrotron Radiation Laboratory, University of Science and Technology of China, Hefei, Anhui 230029, People's Republic of China. [†]Z. Sun and X. Yang contributed equally to this work.

ABSTRACT Control over the magnetic interactions in dilute magnetic semiconductor quantum dots (DMSQDs) is a key issue to future development of nanometer-sized integrated "spintronic" devices. However, manipulating the magnetic coupling between impurity ions in DMSQDs remains a great challenge because of the intrinsic quantum confinement effects and self-purification of the quantum dots. Here, we propose a hybrid structure to achieve room-temperature ferromagnetic interactions in DMSQDs, *via* engineering the density and nature of the energy states at the Fermi level. This idea has been applied to Co-doped ZnO DMSQDs where the growth of a reduced graphene oxide shell around the $Zn_{0.98}Co_{0.02}O$ core turns the magnetic interactions from paramagnetic to ferromagnetic at room temperature, due to the hybridization of $2p_z$ orbitals of graphene and 3d obitals of Co^{2+}—oxygen-vacancy complexes. This design may open up a kind of possibility for manipulating the magnetism of doped oxide nanostructures.

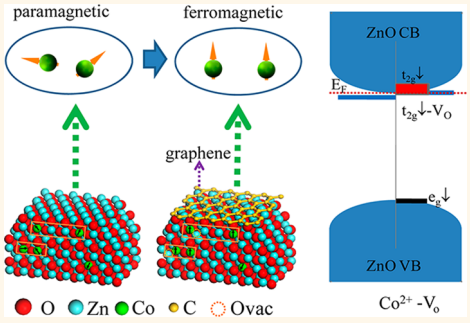

KEYWORDS: Co-doped ZnO QDs · XAFS · RGO · ferromagnetic exchange

Realizing ferromagnetic interactions in dilute magnetic semiconductor quantum dots (DMSQDs) is a central theme to the development of next-generation spin-based information technologies.[1−8] In conventional bulk dilute magnetic semiconductors (DMSs), an effective route to tailor the interactions between magnetic ions is to introduce itinerant or localized carriers *via* a variety of methods.[9] However, ferromagnetic couplings between doped magnetic ions in DMSQDs are usually suppressed[10] due to the quantum confinement that induces p-character (s-character) of the electron (hole) carriers. On the experimental side, the routinely used methods to introduce carriers in bulk DMSs, such as co-doping or annealing under different atmospheres, are hardly applicable for DMSQDs, because of the self-purification or size growth of the quantum dots (QDs) in the heating process.[11] Therefore, it still remains a subject of active investigations to find effective ways for tailoring the magnetic couplings between magnetic ions in DMSQDs. To this goal, significant progress has been made recently, for example, light-induced spontaneous magnetization[12] and charge-controlled magnetism reported in doped colloidal quantum dots.[3] Unfortunately, these methods could not realize the intrinsic ferromagnetic interactions in the materials, and more ways capable of tailoring the inherent magnetic coupling in DMSQDs are still to be developed.

The exchange interactions between magnetic impurities in DMSs are known to rely on the density and nature of the energy states at the Fermi level, which can change the range, strength, and sign of the interactions.[13] Taking into account the small size, large specific surface area, and complex surface states of DMSQDs, the magnetic exchange interactions in DMSQDs cores are anticipated to be tunable *via* surface modifications that change the electronic band structure of DMSQDs. An effective way to change the electronic states of

* Address correspondence to ywsh2000@ustc.edu.cn; qhliu@ustc.edu.cn; sqwei@ustc.edu.cn.

Received for review July 23, 2014 and accepted September 15, 2014.

Published online September 15, 2014
10.1021/nn5040845

DMSQDs is to cover shell materials with electronic properties different from the semiconductor host. Our group has successfully utilized a semiconductor heterostructure to reduce the relative position of Co^{2+} 3d energy levels that alternates the magnetic interactions in ZnO quantum dots and observed ferromagnetic couplings between Co^{2+} at low temperature.[14] Compared with semiconductor shell materials, graphene has unsaturated π orbitals (p_z) and lacks a band gap; both characters are beneficial to electronic interactions with 3d orbitals of transition-metal ions. Moreover, the formation of strong covalent bonds[15−17] between graphene and DMSQDs could steadily pin the DMSQDs on the surface of graphene and avoid migration or evaporation of magnetic ions in this hybrid system. Therefore, graphene is a promising material to effectively change the electronic band structure of DMSQDs and to promote the room-temperature ferromagnetic interactions among magnetic ions, which are essential for applications of DMSQDs in spintronic devices.[18] More importantly, the resulting new DMSQDs−graphene hybrids might possess some unique properties of graphene such as long spin coherence lifetimes and lengths, due to the small spin−orbit coupling ($\sim 10^{-4}$ eV) strength and limited hyperfine interactions. It is then highly predictable that such a category of hybrid material, which possesses the character of both DMS and graphene, offers an unprecedented platform for the advent of spintronics for a complete integration of spin injection, manipulation, and detection.

In this work, we propose that a deliberately designed hybrid structure provides a route to realize room-temperature ferromagnetic couplings in DMSQDs, by engineering the density and nature of the energy states at the Fermi level in DMSQDs. Experimentally, by fully covering Co-doped ZnO DMSQDs (Co-doped ZnO/RGO) with a reduced graphene oxide (RGO) shell, we realize the paramagnetic-to-ferromagnetic transformation of magnetic interactions between Co ions in the Co-doped ZnO DMSQDs system, with the ferromagnetic coupling persisting up to room temperature. The detailed experimental and theoretical results demonstrate that the Co^{2+}−V_O (oxygen vacancy) complex introduced by RGO expands the Co^{2+} empty $t_{2g}{\downarrow}$ minority state and forms an impurity band of $t_{2g}{\downarrow}$−V_O; this is the key factor that results in the room-temperature ferromagnetic interaction between Co^{2+} ions. Our delicate design of the hybrid structure sheds new light on effective manipulation of exchange interactions between magnetic impurities in doped oxide nanostructures for future spintronic applications.

RESULTS AND DISCUSSION

To understand the influence of RGO on the magnetic property of Co-doped ZnO QDs, we have designed and prepared three distinct samples as shown in Figure 1a, namely, $Zn_{0.98}Co_{0.02}O$, $Zn_{0.98}Co_{0.02}O$-RGO, and $Zn_{0.98}Co_{0.02}O$/RGO quantum dots. $Zn_{0.98}Co_{0.02}O$/RGO refers to a quasi-core/shell structure in which the $Zn_{0.98}Co_{0.02}O$ cores are almost fully covered by RGO shells, and $Zn_{0.98}Co_{0.02}O$-RGO means $Zn_{0.98}Co_{0.02}O$ QDs anchored on RGO sheets but not completely wrapped. The synthetic strategy for the $Zn_{0.98}Co_{0.02}O$/RGO is summarized graphically in the Supporting Information (Figure S1). Graphene oxide (GO) was first prepared by surface treatment of natural graphite powder with a mixed acid of H_2SO_4 and HNO_3. Thereafter, in a mixture of zinc acetate dihydrate, cobalt acetate tetrahydrate, and GO in dimethylformamide (DMF), embryo Co-doped ZnO quantum dots were preferentially formed, growing to 6 nm in diameter. $Zn_{0.98}Co_{0.02}O$-RGO was prepared by ultraviolet (UV) irradiation on $Zn_{0.98}Co_{0.02}O$ and GO in ethanol solvent. $Zn_{0.98}Co_{0.02}O$ quantum dots were synthesized using a sol−gel-like method as reported in the literature.[19,20] Since covering $Zn_{0.98}Co_{0.02}O$ QDs with RGO slightly increases their size, to make sure that $Zn_{0.98}Co_{0.02}O$/RGO and $Zn_{0.98}Co_{0.02}O$ have similar sizes, we first synthesized the $Zn_{0.98}Co_{0.02}O$/RGO sample and measured its size. Then by deliberately controlling the reaction conditions of synthesizing $Zn_{0.98}Co_{0.02}O$, we obtained $Zn_{0.98}Co_{0.02}O$ QDs with a size similar to that of $Zn_{0.98}Co_{0.02}O$/RGO. For both $Zn_{0.98}Co_{0.02}O$-RGO and $Zn_{0.98}Co_{0.02}O$/RGO, the Bragg peaks corresponding to the wurtzite structure (ZnO) and graphene are observed simultaneously in the XRD patterns (Supporting Information, Figure S2), indicating that the consolidated $Zn_{0.98}Co_{0.02}O$ and graphene hybrid structures have been successfully synthesized. A typical transmission electron microscopy (TEM) image of $Zn_{0.98}Co_{0.02}O$-RGO is given in Figure 1b. Seen from high-resolution TEM (HRTEM) images shown in the inset, both $Zn_{0.98}Co_{0.02}O$ QDs and the edge of RGO are evident, verifying efficient attachment of $Zn_{0.98}Co_{0.02}O$ QDs on the RGO. Strikingly, the HRTEM image of $Zn_{0.98}Co_{0.02}O$/RGO clearly shows that the outer shell of the $Zn_{0.98}Co_{0.02}O$ QDs is RGO, similar to the results reported by Son *et al.*[21] Judged from the HRTEM image, we can estimate the thickness of the RGO layer to be ~1 nm, *i.e.*, close to those of RGO reported in the literature.[22,23] These results indicate the formation of the quasi-core/shell structure of $Zn_{0.98}Co_{0.02}O$ QDs covered by RGO. Furthermore, the TEM images show spherical particles of $Zn_{0.98}Co_{0.02}O$ with average sizes of ~6 nm for all three samples of $Zn_{0.98}Co_{0.02}O$, $Zn_{0.98}Co_{0.02}O$-RGO, and $Zn_{0.98}Co_{0.02}O$/RGO, and the sizes are in agreement with the values estimated from X-ray diffraction (XRD).

The magnetization measurement results for these nanostructures are displayed in Figure 1c. For $Zn_{0.98}Co_{0.02}O$ QDs, the magnetic-field dependence of magnetization (M−H curve) at 300 K shows a linear relationship between magnetic field and magnetization,

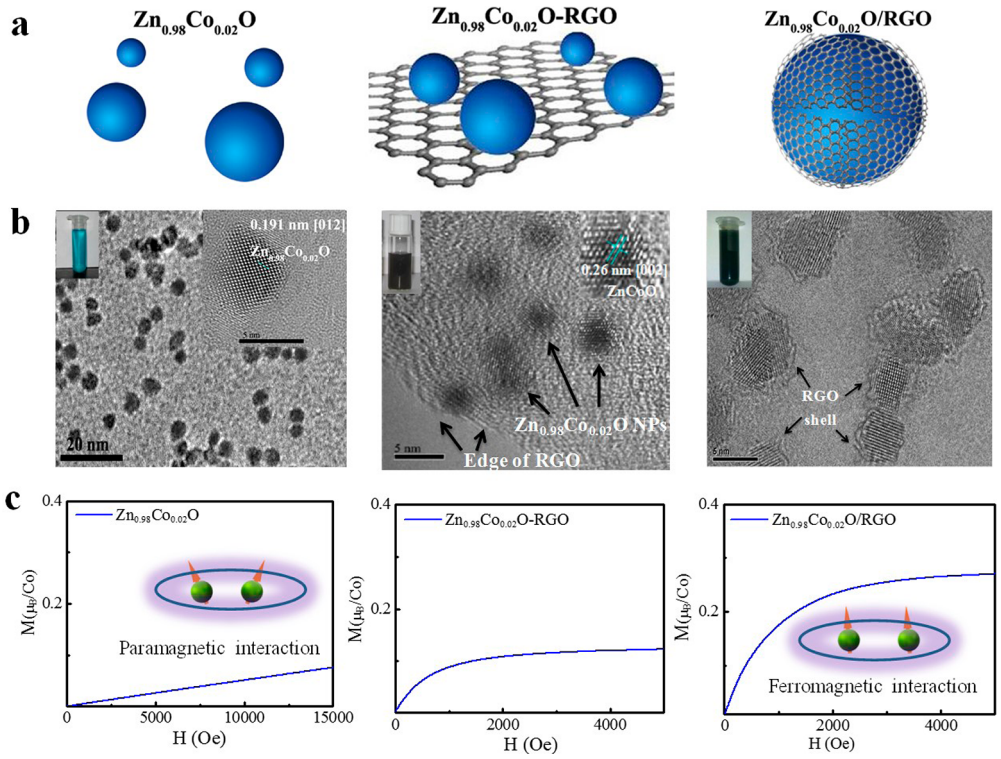

Figure 1. Diagrammatic representation of the synthesis of the DMSQDs−graphene hybrids, characterization of their morphology and magnetic properties. (a) Schematic representation of various $Zn_{0.98}Co_{0.02}O$ and RGO hybrids. (b) TEM images of representative $Zn_{0.98}Co_{0.02}O$, $Zn_{0.98}Co_{0.02}O$-RGO, and $Zn_{0.98}Co_{0.02}O$/RGO quantum dots. The right inset shows a high-resolution TEM image of a single quantum dot. The left insets display the colors of $Zn_{0.98}Co_{0.02}O$, $Zn_{0.98}Co_{0.02}O$-RGO, and $Zn_{0.98}Co_{0.02}O$/RGO suspensions in ethanol. (c) Field dependence of magnetization ($M-H$ curve) of $Zn_{0.98}Co_{0.02}O$, $Zn_{0.98}Co_{0.02}O$-RGO, and $Zn_{0.98}Co_{0.02}O$/RGO (300 K). The insets display the magnetic interactions between Co ions.

i.e., a typical character of paramagnetism. The magnetization *vs* temperature ($M-T$) curve of the $Zn_{0.98}Co_{0.02}O$ QDs further demonstrates that within the temperature range of 0−300 K the paramagnetic interaction still dominates in most of the Co ions and no ferromagnetic coupling is observed (Supporting Information, Figure S3). Furthermore, the inset of Figure S3a shows that the $Zn_{0.98}Co_{0.02}O$ QDs exhibit a Curie−Weiss behavior. We depict the inverse of susceptibility ($1/M$) as a function of temperature under an applied field of 100 Oe. From the high-temperature linear part an extrapolated Curie temperature of about −60 K could be obtained, which indicates that magnetic interactions between the remnant Co ions are antiferromagnetic, a phenomenon similar to that observed by Balcells *et al.* on Co-doped ZnO nanoparticles.[24] These magnetic measurement results are consistent with the widely accepted magnetic character of the doped magnetic ions at low doping level.[25] It is worth noting that at room temperature the Co ions with antiferromagnetic character may exhibit paramagnetic interaction due to the temperature effect. After covering the RGO shell, the $Zn_{0.98}Co_{0.02}O$/RGO QDs exhibit a room-temperature ferromagnetic behavior, as demonstrated by the hysteresis loops (Supporting Information, Figure S3b) as well as by the ($M-H$) field dependence of the magnetization curve under a saturation magnetization at 3000 Oe (right panel of Figure 1c). A similar phenomenon is also observed in $Zn_{0.98}Co_{0.02}O$-RGO, but its saturation magnetic moment (0.1 μ_B/Co) is evidently smaller than that of $Zn_{0.98}Co_{0.02}O$/RGO (the origin of the difference will be discussed later). Since these three samples have very close particle sizes as mentioned above, the differences in their magnetic interactions could not be attributed to the size effects, but to the critical role of the RGO in tuning the magnetic properties of the $Zn_{0.98}Co_{0.02}O$. It is worthy of note that in $Zn_{0.98}Co_{0.02}O$-RGO and $Zn_{0.98}Co_{0.02}O$/RGO the saturation magnetic moment of Co^{2+} is lower than the theoretically calculated value of 3.0 μ_B/Co for Co^{2+} in a tetragonal ligand field, because a considerable amount of Co^{2+} ions still retain paramagnetic or even antiferromagnetic coupling and do not contribute to the saturation magnetization of the samples.

It should be noted that if Co ions are not incorporated simultaneously, RGO alone could not lead to such significant changes of the magnetic interactions in ZnO. To demonstrate this point explicitly, we also synthesized ZnO and ZnO/RGO QDs using the same methods as those for the Co-doped counterparts. The magnetization measurements show that after hybridization with RGO the ZnO QDs do not exhibit a ferromagnetic response, but a diamagnetic behavior (Supporting Information, Figure S4). This suggests that the magnetic changes of $Zn_{0.98}Co_{0.02}O$, $Zn_{0.98}Co_{0.02}O$-RGO,

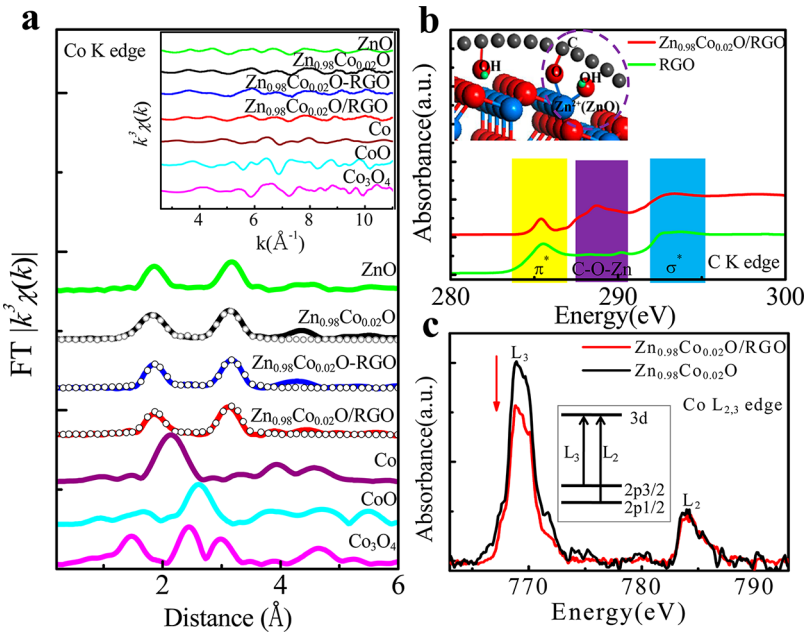

Figure 2. Local structure and electronic structure in DMSQDs−graphene hybrids. (a) Fourier transform of the Co K-edge EXAFS $k^3\chi(k)$ functions for $Zn_{0.98}Co_{0.02}O$-RGO, $Zn_{0.98}Co_{0.02}O$/RGO, $Zn_{0.98}Co_{0.02}O$, Co, CoO, and Co_3O_4. The inset displays the $k^3\chi(k)$ functions. The empty circles show the fitting results. (b) C K-edge XANES spectra of RGO, $Zn_{0.98}Co_{0.02}O$-RGO, and $Zn_{0.98}Co_{0.02}O$/RGO. The inset displays the bonds between RGO and Co-doped ZnO. (c) Co $L_{2,3}$-edge XANES spectra of $Zn_{0.98}Co_{0.02}O$ and $Zn_{0.98}Co_{0.02}O$/RGO. The inset displays the photoelectron transitions of L_3 and L_2 at the Co $L_{2,3}$-edge.

and $Zn_{0.98}Co_{0.02}O$/RGO are tightly correlated with the doped Co ions rather than coming from the modified electronic structures of ZnO QDs or RGO.

In order to clarify that the Co ions are in the substitutional sites for Zn atoms of ZnO rather than in Co-related secondary phases, the X-ray absorption fine structure (XAFS) technique with element-specific and structure-sensitive features was used to probe the local structures of Co ions in the samples.[26] In Figure 2a we display the Fourier transform (FT) of Co K-edge extended XAFS (EXAFS) $k^3\chi(k)$ functions (inset of Figure 2a) for $Zn_{0.98}Co_{0.02}O$, $Zn_{0.98}Co_{0.02}O$-RGO, and $Zn_{0.98}Co_{0.02}O$/RGO. As references, Zn or Co K-edge functions of standard ZnO, Co, CoO, and Co_3O_4 powders are also plotted. At first, we may rule out the existence of Co metal and cobalt oxides (like CoO and Co_3O_4) in the $Zn_{0.98}Co_{0.02}O$, $Zn_{0.98}Co_{0.02}O$-RGO, and $Zn_{0.98}Co_{0.02}O$/RGO nanocrystals because of their significantly different $k^3\chi(k)$ and FT features from those of the nanocrystals. In addition, the overall oscillation shapes of $Zn_{0.98}Co_{0.02}O$, $Zn_{0.98}Co_{0.02}O$-RGO, and $Zn_{0.98}Co_{0.02}O$/RGO are very close to that of ZnO powders (inset of Figure 2a). Like ZnO, these samples also exhibit two FT peaks located at 1.5 and 2.9 Å, corresponding to Co−O and Co−Zn coordinations, respectively. A quantitative fit of these two peaks (Supporting Information, Table S1) shows a good fitting quality, as indicated by empty circles in Figure 2a, demonstrating the substitution of Co in the ZnO lattice and ruling out the presence of Co-related secondary phases within the detection limit of XAFS, even after hybridizing with RGO.

For understanding how the hybridized RGO influences the magnetic exchange interactions in $Zn_{0.98}Co_{0.02}O$ QDs, we performed X-ray absorption near-edge structure (XANES) measurements (Figure 2b) at the C K-edge to detect their electronic features. The characteristic peaks of C 1s → π^* (~285.5 eV) and C 1s → σ^* (~292.5 eV) transitions are observed in the XANES spectra of RGO, consistent with the results by Liang *et al.*[27] Compared with RGO, the $Zn_{0.98}Co_{0.02}O$/RGO hybrid shows a clearly enhanced intensity of the peak at ~288 eV, most probably due to the binding of oxygen or other species to the carbon atoms in RGO. This suggests the formation of interfacial Zn(Co)−O−C bonds (inset of Figure 2b) in the $Zn_{0.98}Co_{0.02}O$/RGO hybrid.[15,27,28] When the $Zn_{0.98}Co_{0.02}O$ nuclei are formed in the presence of RGO, the positively charged Zn plane can react with the functional groups of RGO. Besides, Zn^{2+} bonded to RGO can combine with the negatively charged oxygen plane of $Zn_{0.98}Co_{0.02}O$ nuclei, leading to the abundant Zn(Co)−O−C bonds at the interface of $Zn_{0.98}Co_{0.02}O$ and RGO.[21,29] Along with the formation of interfacial Zn(Co)−O−C bonds, comparison of the Co $L_{2,3}$-edge XANES spectra of $Zn_{0.98}Co_{0.02}O$ and $Zn_{0.98}Co_{0.02}O$/RGO as displayed in Figure 2c shows that the characteristic peaks at about 770 and 784 eV arising from Co 2p → 3d electron transitions are decreased in intensity after hybridizing RGO. This implies the higher Co 3d electron occupation in $Zn_{0.98}Co_{0.02}O$/RGO, primarily due to the charge transfer from C 1s to Co 3d states. Such a charge transfer could also be inferred from the Co K-edge XANES spectra as displayed in the Supporting

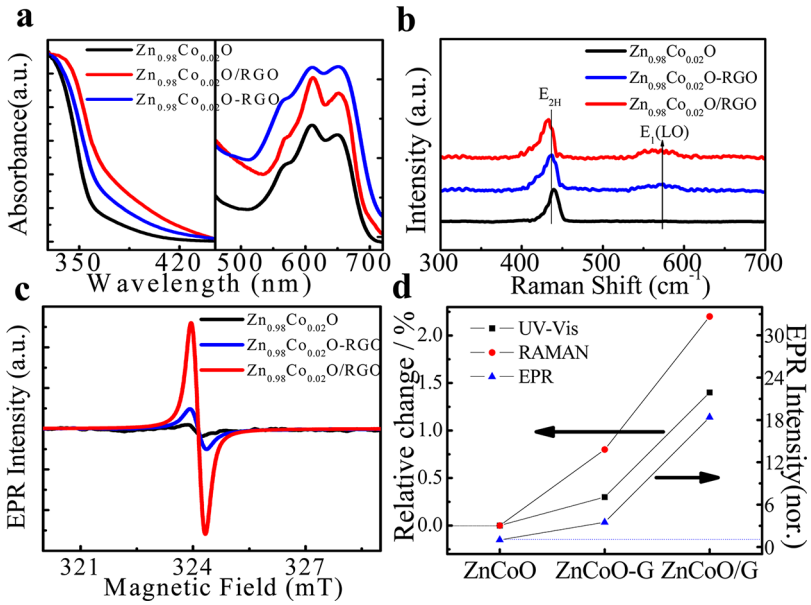

Figure 3. Interactions between the DMSQDs and graphene in the DMSQDs−graphene hybrids. (a) Electronic absorption spectra of $Zn_{0.98}Co_{0.02}O$, $Zn_{0.98}Co_{0.02}O$-RGO, and $Zn_{0.98}Co_{0.02}O$/RGO. (b) Raman spectra of $Zn_{0.98}Co_{0.02}O$, $Zn_{0.98}Co_{0.02}O$-RGO, and $Zn_{0.98}Co_{0.02}O$/RGO. (c) EPR spectra of $Zn_{0.98}Co_{0.02}O$, $Zn_{0.98}Co_{0.02}O$-RGO, and $Zn_{0.98}Co_{0.02}O$/RGO. (d) Summarized change tendencies of electronic absorption spectra, Raman spectra, and EPR spectra along with the hybrid form.

Information (Figure S5). On the basis of these results, we believe that strong electronic interactions and electron transfer are introduced at the interface of RGO and $Zn_{0.98}Co_{0.02}O$. This scenario is also supported by a similar study on the hybrid structure of TiO_2 and RGO, where electron transfer from RGO to TiO_2 is observed.[30]

The influence of the RGO on the band structure of $Zn_{0.98}Co_{0.02}O$ quantum dots could be further revealed by a comparison of the electronic absorption spectra of $Zn_{0.98}Co_{0.02}O$, $Zn_{0.98}Co_{0.02}O$-RGO, and $Zn_{0.98}Co_{0.02}O$/RGO QDs (Figure 3a). All three samples display strong absorption features centered at 2.0 eV that arise from the spin−orbit split ligand-field transition $^4A_2 \rightarrow {}^4T_1(P)$ of tetrahedral Co^{2+}, in agreement with the substitution of Co^{2+} ions at the Zn^{2+} sites in ZnO QDs. The band gap (3.61 eV) of $Zn_{0.98}Co_{0.02}O$ QDs is wider than that of the bulk (3.37 eV) due to the strong quantum confinement. However, after hybridization with RGO, the energy gap of $Zn_{0.98}Co_{0.02}O$ QDs is narrowed, probably because of the strain caused by the interface between ZnO and graphene,[31] which was also observed in the ZnO and graphene oxide platelets hybrid.[32] The red-shift of the characteristic E_{2H} peak (Figure 3b) and 2D peak (Supporting Information, Figure S6) of the Raman spectra also indicates the intensive electron interaction between $Zn_{0.98}Co_{0.02}O$ and RGO, in agreement with the electronic absorption spectra. More interestingly, the electronic paramagnetic resonance (EPR) spectra suggest that after hybridization with RGO the oxygen vacancies (V_O) in the sample are obviously concentrated, as reflected from the intensified EPR signal at 324.1 mT that is proportional to the concentration of oxygen vacancies (Figure 3c).[33,34] The same phenomenon is also observed in the EPR (Supporting Information, Figure S7) and photoluminescence (PL, Supporting Information, Figure S8) spectra of ZnO and ZnO/RGO. Our results are in good agreement with that by Son *et al.*, who also used PL spectra to indicate the increased V_O content of ZnO QDs upon hybridizing RGO.[21] Meanwhile, it is worth noting that Bahadur *et al.* conducted PL measurements on 60 nm ZnO nanoparticles hybridized with RGO and observed reduced V_O content, which was ascribed to the RGO-induced surface passivation.[35,36] A summary of these studies suggests that there might be different mechanisms of RGO influencing V_O in ZnO, and these mechanisms are strongly dependent on the size of the ZnO particles. Detailed investigation of this size effect is beyond the scope of this work.

Putting the above together, we may conclude that the band gap and V_O concentration in $Zn_{0.98}Co_{0.02}O$/RGO and $Zn_{0.98}Co_{0.02}O$-RGO are sensitively dependent on the hybridization form of RGO with Co-doped ZnO QDs, and RGO can effectively tune the electron band structure of $Zn_{0.98}Co_{0.02}O$ (Figure 3d). Especially, the formation of abundant oxygen vacancies would evidently change the density and nature of the states at the Fermi level, quite beneficial for tailoring the magnetic interaction between the magnetic ions. Recently, Song *et al.*[37] and Pan *et al.*[38] manipulated the magnetic properties of the Pt/$Zn_{0.95}Co_{0.05}O$/Pt device by changing the distribution of oxygen vacancy using an external electric field and provided more evidence for the important role of oxygen vacancies in mediating the ferromagnetic ordering of Co:ZnO materials. In spite of the critical role of oxygen vacancies in tuning the electronic structures and properties of the

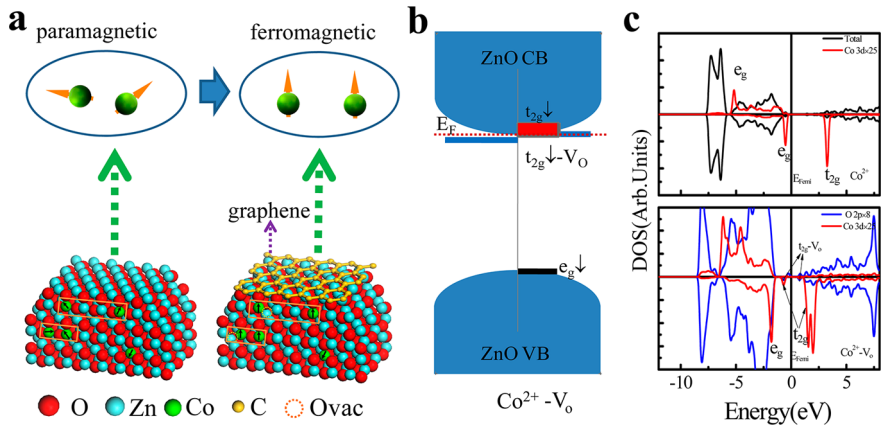

Figure 4. Model structure and calculated electronic structures in DMSQDs−graphene hybrids. (a) Schematic for the hybridization between Co−Co pairs before and after covering the RGO shell (top view). Schematic of the theoretical model for the magnetic interactions between Co ions in different depth layers influenced by the RGO shell (down view). (b) Schematic for electronic band structure of ZnO with V_O (Co^{2+}−V_O) (c) Calculated density of states (DOS) for various model structures: Co ions in ZnO without V_O and Co ions in ZnO with V_O (Co^{2+}−V_O).

ZnO−graphene hybrid structure as seen from the PL (Supporting Information, Figure S8) and EPR (Figure 3c and Supporting Information, Figure S7), it should be emphasized that an oxygen vacancy alone still could not lead to the magnetic changes of the $Zn_{0.98}Co_{0.02}O$, $Zn_{0.98}Co_{0.02}O$-RGO, and $Zn_{0.98}Co_{0.02}O$/RGO. This viewpoint is experimentally strengthened by a comparison of the paramagnetism of ZnO/RGO with the ferromagnetism of $Zn_{0.98}Co_{0.02}O$/RGO at room temperature.

For an in-depth understanding on how oxygen vacancies mediate the Co^{2+}−Co^{2+} magnetic exchange interactions in the $Zn_{0.98}Co_{0.02}O$/RGO hybrids, first-principles energy and electronic structure calculations were performed. The calculation details are included in the Supporting Information. The energy calculations show that after obtaining the RGO shell, the formation energy of V_O in Co-doped ZnO is significantly reduced by about 0.8 eV. This suggests that the RGO shell would result in abundant oxygen vacancies in Co-doped ZnO, as evidenced by the EPR results. The lowered formation energy of V_O is mainly attributed to the electron transfer between RGO and ZnO, which leads to the upshift of Fermi level of ZnO.[39] Our total energy calculations further reveal that V_O prefers to exist as the nearest neighbors of Co to form Co^{2+}−V_O complexes, which is supported by the Co K-edge XANES spectrum and the real-space multiple-scattering theory calculations (Supporting Information, Figure S9). The presence of the Co^{2+}−V_O pairs has also been observed by Ciato *et al.* in Co-doped ZnO thin films grown by the PLD method.[40] Our magnetic coupling energy calculation results suggest that the ferromagnetic interaction between Co−V_O pairs is still preferable even at a large distance of 8.5 Å. In comparison with the single Co^{2+}, Co^{2+}−V_O pairs sustain a long-range ferromagnetic coupling.[41] In other words, with the formation of Co^{2+}−V_O pairs, both the antiferromagnetic interaction between the neighboring Co^{2+} ions and the paramagnetic interaction between the long-range Co^{2+} ions are transformed into the ferromagnetic interaction (Figure 4a). Inferred from the obtained density of states as shown in Figure 4c, such a change in magnetic interactions is intimately related to modifications of the electronic structures. Seen from Figure 4c, the tetrahedral symmetry around Co atoms splits the Co 3d levels into a doubly degenerate e_g band and a triply degenerate t_{2g} band. All the Co^{2+} spin-up 3d levels are covalently delocalized into the valence band of ZnO semiconductor host, but the spin-down $t_{2g}\downarrow$ level is remarkably higher in energy than the edge of CB. As V_O coexists with the nearest Co^{2+} (Co^{2+}−V_O pairs), the Co^{2+} empty $t_{2g}\downarrow$ minority state broadens and forms a hybrid level ($t_{2g}\downarrow$−V_O) right at the CBM as shown in Figure 4b,c. This extends in space over the first shell of Zn ions, and an impurity band forms already at trace concentrations, favoring the strong ferromagnetic coupling between Co^{2+} ions. Furthermore, Figure 4c indicates a portion of electrons occupying the $t_{2g}\downarrow$ state of the Co−V_O pairs. This is due to the hybridization of the RGO $2p_z$ state and Co^{2+} 3d state, leading to partial electron transfer of RGO π electrons to the Co^{2+} 3d states and promoting the ferromagnetic interaction between the Co^{2+}−V_O pairs.[41] In fact, the evident reduction of the Co $L_{2,3}$ characteristic peak confirms the electron transfer from RGO to ZnO (Figure 2c). Therefore, the macroscopical magnetic measurement results demonstrate that ferromagnetic interactions between Co^{2+} ions are induced after the hybridization of $Zn_{0.98}Co_{0.02}O$ and RGO.

Finally, we compare the difference of ZnCoO-RGO and ZnCoO/RGO, both of which are a hybrid structure between ZnCoO and RGO. As schematically shown in Figure 1a, the ZnCoO quantum dots are almost fully wrapped by RGO in ZnCoO/RGO, while partly wrapped in ZnCoO-RGO. Compared with ZnCoO-RGO, ZnCoO/RGO has a much higher extent of hybridization and

contains more Co(Zn) atoms interacting with C atoms, leading to higher V_O content and more Co^{2+}—V_O pairs. As the formation of Co^{2+}—V_O pairs is favorable to the ferromagnetic interactions in $Zn_{0.98}Co_{0.02}O$ QDs, the saturation magnetization of $Zn_{0.98}Co_{0.02}O$/RGO is significantly larger than that of $Zn_{0.98}Co_{0.02}O$-RGO (Figure 1c). It is worth noting that as V_O moves apart from the graphene shell, the formation energy of V_O increases. This suggests that the Co^{2+}—V_O pairs introduced by graphene mainly locate at the near surface area of $Zn_{0.98}Co_{0.02}O$ QDs. Taking into account the much smaller saturation magnetization moment of $Zn_{0.98}Co_{0.02}O$ QDs than the theoretical value (0.1—0.3 *vs* 3 μ_B/Co), it could be inferred that the dominant Co^{2+}—Co^{2+} interactions in the central part of the QDs are still antiferromagnetic or paramagnetic.

CONCLUSIONS

In summary, using the Co-doped ZnO system as an example, we demonstrate that engineering the density and nature of the electronic states at the Fermi level of DMSQDs *via* a hybrid structure is an effective way to tune the magnetic interactions between the impurity ions. As shown by a detailed study of structural and magnetic properties, this concept is applicable to $Zn_{0.98}Co_{0.02}O$, $Zn_{0.98}Co_{0.02}O$-RGO, and $Zn_{0.98}Co_{0.02}O$/RGO. Through the comparison of Co-doped ZnO/RGO with Co-doped ZnO QDs and Co-doped ZnO-RGO, it is revealed that RGO introduces a Co^{2+}—V_O complex in Co-doped ZnO because of the electron transfer from RGO to Co-doped ZnO. The formation of a Co^{2+}—V_O complex broadens the Co^{2+} empty $t_{2g}\downarrow$ minority state and introduces an impurity energy band of $t_{2g}\downarrow$—V_O at the conduction band minimum (CBM), which is responsible for the observed room-temperature ferromagnetic interaction between Co^{2+} ions in the hybrid structure of Co-doped ZnO and RGO. These experimental results also shed new light on the role of shell growth in modifying the dopant—dopant magnetic exchange interactions in colloidal doped core/shell quantum dots. They also raise new questions and challenges regarding the role of functional doping ions and defect pairs in altering fundamental mechanisms such as the dopant—carrier magnetic exchange coupling in semiconductor nanostructures.

METHODS

Synthesis of Different Samples. Graphene oxide was synthesized from natural graphite by the modified Hummer's method. $Zn_{0.98}Co_{0.02}O$ NPs were prepared from cobalt acetate tetrahydrate and zinc acetate dihydrate using the coprecipitation method. $Zn_{0.98}Co_{0.02}O$-RGO composite was obtained by the UV-irradiating process, which can realize the reduction of GO. $Zn_{0.98}Co_{0.02}O$/RGO quasi-core—shell structure was prepared by a simple two-step solution method. Details can be found in the Supporting Information.

Structure and Property Characterization. Dopant concentrations were examined by inductively coupled plasma atomic emission spectrometry (ICP-AES Jarrel Ash model 955). Morphology and size of the prepared samples were observed using a JEM-2100 microscope operated at 200 kV (JEOL Co., Japan). UV—vis absorbance spectra were measured using a TU-1901 UV—vis spectrophotometer (Persee Co., China). The crystal structures were investigated *via* an X'Pert PRO X-ray diffractometer (Philips, The Netherlands). Raman and PL spectra were recorded by a JobinYvon LABRAM-HR Raman spectrometer system with a 514.5 nm excitation source and FLUOROLOG-3-TAU steady life fluorescent spectrometer, respectively. The C K-edge X-ray absorption near-edge spectra were measured at beamline U19 of National Syncrotron Radiation Laboratory (NSRL, China) in the total electron yield (TEY) mode by collecting the sample drain current under a vacuum better than 5×10^{-6} Pa. The beam from the bending magnet was monochromatized utilizing a varied line-spacing plane grating and refocused by a toroidal mirror. The energy range is 100—1000 eV with an energy resolution of *ca.* 0.2 eV. The Co K-edge XAFS spectra were recorded at the U7C beamline of NSRL, the 1W1B beamline of Beijing Syncrotron Radiation Facility (BSRF, China), and the BL14W1 beamline of Shanghai Syncrotron Radiation Facility (SSRF, China). The electron-beam energy of NSRL was 0.8 G eV, and the stored current was from 250 to 300 mA. The storage ring of BSRF worked at 2.5 GeV with a maximum current of 250 mA, and the ring of SSRF at 3.5 GeV and current of 210 mA. The Co $L_{2,3}$-edge X-ray absorption fine structure data were obtained at the BL08U beamline of SSRF in the TEY mode. Magnetic data were collected with a Quantum Design MPMS-5 superconducting quantum interference device (SQUID) magnetometer. Electronic paramagnetic resonance spectra were recorded using a JSE-FA200 EPR spectrometer at X-band (~9 GHz) at room temperature.

Conflict of Interest: The authors declare no competing financial interest.

Acknowledgment. This work was supported by the National Basic Research Program of China (2012CB825800), National Natural Science Foundation of China (Grant Nos. 11435012, U1332131, 11135008, 11175184, 11305172, U1332111, 11422547), and New Century Excellent Talents in Chinese University. The authors are grateful to NSRL, BSRF, and SSRF for the valuable beamtime.

Supporting Information Available: XRD patterns, *M*—*T* curves, Raman spectra, comparison between experimental XANES spectra, XAFS measurement and data analysis, and density functional theory calculation details and analysis. This material is available free of charge *via* the Internet at http://pubs.acs.org.

REFERENCES AND NOTES

1. Erwin, S. C.; Zu, L.; Haftel, M. I.; Efros, A. L.; Kennedy, T. A.; Norris, D. J. Doping Semiconductor Nanocrystals. *Nature* **2005**, *436*, 91–94.
2. Bussian, D. A.; Crooker, S. A.; Yin, M.; Brynda, M.; Efros, A. L.; Klimov, V. I. Tunable Magnetic Exchange Interactions in Manganese-Doped Inverted Core-Shell ZnSe-CdSe Nanocrystals. *Nat. Mater.* **2009**, *8*, 35–40.
3. Ochsenbein, S. T.; Feng, Y.; Whitaker, K. M.; Badaeva, E.; Liu, W. K.; Li, X. S.; Gamelin, D. R. Charge-Controlled Magnetism in Colloidal Doped Semiconductor Nanocrystals. *Nat. Nanotechnol.* **2009**, *4*, 681–687.
4. Viswanatha, R.; Pietryga, J.; Klimov, V.; Crooker, S. Spin-Polarized Mn^{2+} Emission from Mn-Doped Colloidal Nanocrystals. *Phys. Rev. Lett.* **2011**, *107*, 067402.
5. Bradshaw, L. R.; May, J. W.; Dempsey, J. L.; Li, X.; Gamelin, D. R. Ferromagnetic Excited-State Mn^{2+} Dimers in $Zn_{1-x}Mn_xSe$ Quantum Dots Observed by Time-Resolved

Magnetophotoluminescence. *Phys. Rev. B* **2014**, *89*, 115312.
6. Chen, O.; Shelby, D. E.; Yang, Y.; Zhuang, J.; Wang, T.; Niu, C.; Omenetto, N.; Cao, Y. C. Excitation-Intensity-Dependent Color-Tunable Dual Emissions from Manganese-Doped CdS/ZnS Core/Shell Nanocrystals. *Angew. Chem., Int. Ed.* **2010**, *49*, 10132–10135.
7. Gamelin, D. R.; Ochsenbein, S. T. Quantum Oscillations in Magnetically Doped Colloidal Nanocrystals. *Nat. Nanotechnol.* **2011**, *6*, 111–114.
8. Chang, K.; Chan, K.; Peeters, F. Spin-Polarized Tunneling through a Diluted Magnetic Semiconductor Quantum Dot. *Phys. Rev. B* **2005**, *71*, 155309.
9. Sato, K.; Kudrnovský, J.; Dederichs, P. H.; Eriksson, O.; Turek, I.; Sanyal, B.; Bouzerar, G.; Katayama-Yoshida, H.; Dinh, V. A.; Fukushima, T.; *et al*. First-Principles Theory of Dilute Magnetic Semiconductors. *Rev. Mod. Phys.* **2010**, *82*, 1633–1690.
10. Merkulov, I. A.; Yakovlev, D. R.; Keller, A.; Ossau, W.; Geurts, J.; Waag, A.; Landwehr, G.; Karczewski, G.; Wojtowicz, T.; Kossut, J. Kinetic Exchange between the Conduction Band Electrons and Magnetic Ions in Quantum-Confined Structures. *Phys. Rev. Lett.* **1999**, *83*, 1431–1434.
11. Dalpian, G. M.; Chelikowsky, J. R. Self-Purification in Semiconductor Nanocrystals. *Phys. Rev. Lett.* **2006**, *96*, 226802.
12. Beaulac, R.; Schneider, L.; Archer, P. I.; Bacher, G.; Gamelin, D. R. Light-Induced Spontaneous Magnetization in Doped Colloidal Quantum Dots. *Science* **2009**, *325*, 973–976.
13. Fernandez-Rossier, J.; Brey, L. Ferromagnetism Mediated by Few Electrons in a Semimagnetic Quantum Dot. *Phys. Rev. Lett.* **2004**, *93*, 117201.
14. Yan, W.; Liu, Q.; Wang, C.; Yang, X.; Yao, T.; He, J.; Sun, Z.; Pan, Z.; Hu, F.; Wu, Z.; *et al*. Realizing Ferromagnetic Coupling in Diluted Magnetic Semiconductor Quantum Dots. *J. Am. Chem. Soc.* **2014**, *136*, 1150–1155.
15. Liang, Y. Y.; Wang, H. L.; Zhou, J. G.; Li, Y. G.; Wang, J.; Regier, T.; Dai, H. J. Covalent Hybrid of Spinel Manganese-Cobalt Oxide and Graphene as Advanced Oxygen Reduction Electrocatalysts. *J. Am. Chem. Soc.* **2012**, *134*, 3517–3523.
16. Geng, W.; Zhao, X.; Liu, H.; Yao, X. Influence of Interface Structure on the Properties of ZnO/Graphene Composites: A Theoretical Study by Density Functional Theory Calculations. *J. Phys. Chem. C* **2013**, *117*, 10536–10544.
17. Zhu, H. O.; Qin, X. M.; Sun, X.; Yan, W. S.; Yang, J. L.; Xie, Y. Rocking-Chair Configuration in Ultrathin Lithium Vanadate-Graphene Hybrid Nanosheets for Electrical Modulation. *Sci. Rep.* **2013**, *3*, 1246.
18. Huang, B.; Xiang, H. J.; Yu, J. J.; Wei, S. H. Effective Control of the Charge and Magnetic States of Transition-Metal Atoms on Single-Layer Boron Nitride. *Phys. Rev. Lett.* **2012**, *108*, 206802.
19. Yao, T.; Yan, W. S.; Sun, Z. H.; Pan, Z. Y.; He, B.; Jiang, Y.; Wei, H.; Nomura, M.; Xie, Y.; Xie, Y. N.; *et al*. High-Temperature Ferromagnetism of Hybrid Nanostructure Ag-$Zn_{0.92}Co_{0.08}O$ Dilute Magnetic Semiconductor. *J. Phys. Chem. C* **2009**, *113*, 3581–3585.
20. Liu, T.; Xu, H. R.; Chin, W. S.; Yong, Z. H.; Wee, A. T. S. Local Structural Evolution of Co-Doped ZnO Nanoparticles upon Calcination Studied by *in Situ* Quick-Scan XAFS. *J. Phys. Chem. C* **2008**, *112*, 3489–3495.
21. Son, D. I.; Kwon, B. W.; Park, D. H.; Seo, W. S.; Yi, Y.; Angadi, B.; Lee, C. L.; Choi, W. K. Emissive ZnO-Graphene Quantum Dots for White-Light-Emitting Diodes. *Nat. Nanotechnol.* **2012**, *7*, 465–471.
22. Loh, K. P.; Bao, Q. L.; Eda, G.; Chhowalla, M. Graphene Oxide as a Chemically Tunable Platform for Optical Applications. *Nat. Chem.* **2010**, *2*, 1015–1024.
23. Paredes, J. I.; Villar-Rodil, S.; Solis-Fernandez, P.; Martinez-Alonso, A.; Tascon, J. M. D. Atomic Force and Scanning Tunneling Microscopy Imaging of Graphene Nanosheets Derived from Graphite Oxide. *Langmuir* **2009**, *25*, 5957–5968.
24. Martinez, B.; Sandiumenge, F.; Balcells, L.; Arbiol, J.; Sibieude, F.; Monty, C. Structure and Magnetic Properties of Co-Doped ZnO Nanoparticles. *Phys. Rev. B* **2005**, *72*, 165202.
25. Coey, J. M. D.; Wongsaprom, K.; Alaria, J.; Venkatesan, M. Charge-Transfer Ferromagnetism in Oxide Nanoparticles. *J. Phys. D: Appl. Phys.* **2008**, *41*, 134012.
26. Yan, W. S.; Sun, Z. H.; Li, Z. R.; Liu, Q. H.; Yao, T.; Pan, Z. Y.; Wang, C.; Hu, F. C.; Jiang, Y.; Qi, Z. M.; *et al*. Valence State-Dependent Ferromagnetism in Mn-Doped NiO Thin Films. *Adv. Mater.* **2012**, *24*, 353–357.
27. Liang, Y. Y.; Li, Y. G.; Wang, H. L.; Zhou, J. G.; Wang, J.; Regier, T.; Dai, H. J. Co_3O_4 Nanocrystals on Graphene as a Synergistic Catalyst for Oxygen Reduction Reaction. *Nat. Mater.* **2011**, *10*, 780–786.
28. Wang, J.; Zhou, J.; Hu, Y. F.; Regier, T. Chemical Interaction and Imaging of Single Co_3O_4/Graphene Sheets Studied by Scanning Transmission X-Ray Microscopy and X-Ray Absorption Spectroscopy. *Energy Environ. Sci.* **2013**, *6*, 926–934.
29. Kavitha, M. K.; John, H.; Gopinath, P.; Philip, R. Synthesis of Reduced Graphene Oxide—ZnO Hybrid with Enhanced Optical Limiting Properties. *J. Mater. Chem. C* **2013**, *1*, 3669–3676.
30. Lee, J. S.; You, K. H.; Park, C. B. Highly Photoactive, Low Bandgap TiO_2 Nanoparticles Wrapped by Graphene. *Adv. Mater.* **2012**, *24*, 1084–1088.
31. Schrier, J.; Demchenko, D. O.; Wang, L. W.; Alivisatos, A. P. Optical Properties of ZnO/ZnS and ZnO/ZnTe Heterostructures for Photovoltaic Applications. *Nano Lett.* **2007**, *7*, 2377–2382.
32. Ahmad, M.; Ahmed, E.; Hong, Z. L.; Xu, J. F.; Khalid, N. R.; Elhissi, A.; Ahmed, W. A Facile One-Step Approach to Synthesizing ZnO/Graphene Composites for Enhanced Degradation of Methylene Blue under Visible Light. *Appl. Surf. Sci.* **2013**, *274*, 273–281.
33. Pan, X. Y.; Yang, M. Q.; Xu, Y. J. Morphology Control, Defect Engineering and Photoactivity Tuning of ZnO Crystals by Graphene Oxide - A Unique 2D Macromolecular Surfactant. *Phys. Chem. Chem. Phys.* **2014**, *16*, 5589–5599.
34. Jakes, P.; Erdem, E. Finite Size Effects in ZnO Nanoparticles: An Electron Paramagnetic Resonance (EPR) Analysis. *Phys. Status Solidi RRL* **2011**, *5*, 56–58.
35. Prakash, A.; Bahadur, D. The Role of Ionic Electrolytes on Capacitive Performance of ZnO-Reduced Graphene Oxide Nanohybrids with Thermally Tunable Morphologies. *ACS Appl. Mater. Interfaces* **2014**, *6*, 1394–1405.
36. Prakash, A.; Misra, S. K.; Bahadur, D. The Role of Reduced Graphene Oxide Capping on Defect Induced Ferromagnetism of ZnO Nanorods. *Nanotechnology* **2013**, *24*, 095705.
37. Chen, G.; Song, C.; Chen, C.; Gao, S.; Zeng, F.; Pan, F. Resistive Switching and Magnetic Modulation in Cobalt-Doped ZnO. *Adv. Mater.* **2012**, *24*, 3515–3520.
38. Pan, F.; Gao, S.; Chen, C.; Song, C.; Zeng, F. Recent Progress in Resistive Random Access Memories: Materials, Switching Mechanisms, and Performance. *Mater. Sci. Eng., R* **2014**, *83*, 1–59.
39. Lany, S.; Zunger, A. Dopability, Intrinsic Conductivity, and Nonstoichiometry of Transparent Conducting Oxides. *Phys. Rev. Lett.* **2007**, *98*, 045501.
40. Ciatto, G.; Di Trolio, A.; Fonda, E.; Alippi, P.; Testa, A.; Bonapasta, A. Evidence of Cobalt-Vacancy Complexes in $Zn_{1-x}Co_xO$ Dilute Magnetic Semiconductors. *Phys. Rev. Lett.* **2011**, *107*, 127206.
41. Pemmaraju, C. D.; Hanafin, R.; Archer, T.; Braun, H. B.; Sanvito, S. Impurity-Ion Pair Induced High-Temperature Ferromagnetism in Co-Doped ZnO. *Phys. Rev. B* **2008**, *78*, 054428.